Environmental Technology & Innovation 43 (2026) 105039

Contents lists available at ScienceDirect

Environmental Technology & Innovation

journal homepage: www.elsevier.com/locate/eti

Tramadol degradation by high-energy ionizing radiation: A study on radical reactions and matrix effects

Krisztina Kovács [a,*], Anna Tegze [a], Anikó Bezsenyi [b,c], László Wojnárovits [a]

[a] HUN-REN Centre for Energy Research, Institute for Energy Security and Environmental Safety, Surface Chemistry and Catalysis Department, Radiation Chemistry Group, Konkoly-Thege Miklós út 29-33, Budapest 1121, Hungary
[b] Institute of Environmental Engineering and Natural Sciences, Rejtő Sándor Faculty of Light Industry and Environmental Engineering, Óbuda University, Doberdó u. 6., Budapest 1034, Hungary
[c] Budapest Sewage Works Pte Ltd., Asztalos Sándor út 4., Budapest 1087, Hungary

ARTICLE INFO

Keywords:
Tramadol
Degradation mechanism
Effect of protonation
•OH reaction
Matrix effects

ABSTRACT

Tramadol, a widely used opioid analgesic, has been detected as an emerging contaminant in both surface waters and wastewaters. Its removal during conventional wastewater treatments is incomplete resulting at concentrations from the ng dm^{-3} range up to the low μg dm^{-3} range in municipal wastewater treatment plant effluents in many countries. This study provides a detailed investigation of tramadol degradation under high-energy ionizing radiation conditions, with emphasis on hydroxyl radical (•OH) reactions and the impact of matrix on removal efficiency. The pK_a of Tramadol (9.41) plays a major role in •OH reactions. Below pK_a the predominant pathway is •OH addition to the aromatic ring, whereas above pK_a, the reactions at the amino group have also high yield *via H*-abstraction from the *C*-atoms next to *N*. For the interpretation of matrix effect on the removal efficiency of Tramadol, degradation in ultrapure water, tap water, synthetic wastewater, and treated wastewater matrices were investigated. Oxidation was clearly observed, while mineralization was more limited, and the biodegradability continuously increased with the absorbed doses. In the standard *Vibrio fischeri* bioassays the fluorescence inhibition of both the parent compound and its degradation products remained below 20% in pure water. The matrix constituents like organic and inorganic matters, metal ions acted as radical scavengers and reduced the efficiency of irradiation. From the technological perspective, high-energy ionizing radiation proved effective to disrupt the molecular structure of Tramadol, thereby decreasing its environmental impact.

1. Introduction

The prevalence of emerging micropollutants including pharmaceuticals, personal care products, and industrial chemicals may pose significant environmental challenges due to their presence in various aquatic environments, persistence and limited removal by conventional wastewater treatment processes. In Europe, the Water Framework Directive (Directive, 2000/60/EC n.d.) and the Urban Wastewater Treatment Directive (Council Directive 91/271/EEC n.d.) provide legal frameworks for water quality management. According to the directive, by 31 December 2045, all urban waste water treatment plants with a load of more than 150,000 Population Equivalent (PE) must achieve an adequate (80%) removal efficiency for micropollutants, but the regulation also affects smaller waste

* Corresponding author.
E-mail address: kovacs.krisztina@ek.hun-ren.hu (K. Kovács).

https://doi.org/10.1016/j.eti.2026.105039
Received 2 April 2026; Received in revised form 1 June 2026; Accepted 11 June 2026
Available online 11 June 2026

water treatment plants where the concentration or accumulation of micropollutants in the water body receiving the treated effluent poses a risk to human health or the environment (e.g. catchment areas of water abstraction points intended for human consumption). Therefore, new technological units are expected to be installed at wastewater treatment plants across Europe, particularly as tertiary or polishing treatment steps. Among these, Advanced Oxidation Processes (AOPs), for example ozone treatment, are considered among the most promising options. Consequently, further research in this field remains highly relevant.

Tramadol ((±) trans−2-[(dimethylamino) methyl]−1-(3-methoxyphenyl)-cyclohexanol, TRA) is a centrally acting analgesic drug (Sarkany et al., 2019) used for reduction of acute or chronic pain (Subedi et al., 2019) as a racemic mixture of its trans enantiomers: (1 *R*, 2 *R*) and (1*S*, 2*S*) (Fig. 1.). The *N*-atom undergoes protonation/deprotonation equilibrium with a pK_a of 9.41.

Tramadol is listed among the top 100 pharmaceuticals used in the clinical practice and has become one of the most frequently prescribed opioid analgesics (Patel et al., 2019). Compared with classical opioids such as morphine, TRA is generally considered to have a lower incidence of severe opioid-related adverse effects when used at therapeutic doses. However, clinically relevant risks remain, particularly in cases of overdose or combined exposure with alcohol and other central nervous system depressants. TRA overdose may increases the risk of seizures, it is also contraindicated in patients with acute alcohol intoxication or severe central nervous system/respiratory depression (Subedi et al., 2019; Manouchehri et al., 2023).

Following the oral administration, TRA is rapidly absorbed, with an estimated bioavailability of 65 – 70% as a result of extensive first-pass hepatic metabolism (Patel et al., 2019). Its two main metabolites are *O*-desmethyltramadol possessing an analgesic effect and *N*-desmethyltramadol. Its un-metabolized fraction entering sewage after being ingested and subjected to human metabolism is approximately 10 – 30% (Ardakani and Rouini, 2007). In the conventional wastewater treatment plants (WWTPs) it is only partially removed. For example, Rúa-Gómez et al. (2012) reported a maximum removal efficiency of 41% for TRA during conventional treatment. Consistent with this limited removal, the authors detected tramadol in WWTP effluents treating household and hospital wastewater at a mean concentration of 757 ng dm^{-3}, while concentrations in receiving surface waters ranged from below the limit of quantification (<LOQ) to 381 ng dm^{-3}. Similarly, tramadol concentrations of 88–416 ng dm^{-3} were reported after activated sludge treatment. Consistently, TRA has frequently been detected in WWTP effluents and surface waters from the ng dm^{-3} level to the low μg dm^{-3} in some samples (Antonopoulou et al., 2016a; Antonopoulou, Konstantinou 2016b; Verlicchi et al., 2012). Because of its low n-octanol/water partition coefficient log K_{ow} (3.01) shows a tendency to persist in the aqueous phase rather than to accumulate in sewage sludge or aquatic organisms (Moustafa et al., 2020). Kostanjevecki et al. (2019) noted that TRA is classified as one of the extremely recalcitrant micropollutants. In the literature published environmental monitoring data indicate that tramadol may also be toxicologically relevant: TRA posed a moderate risk to the assessed organisms at three trophic levels (Sadutto et al., 2021). Pharmaceutical residues and their metabolites may have an unfavourable impact on fish and other aquatic biota (Plhalova et al., 2020; Subedi et al., 2019).

Recently Advanced Oxidation Processes (AOPs), based on reactions of aggressive free radical reactions (Stephan, 2018) are extensively investigated in order to remove the recalcitrant compounds from the streams of purified wastewater. In most of AOPs hydroxyl radicals ($^{\bullet}$OH) play the key role in initiating the degradation of pollutants. Such AOPs in which TRA degradation was investigated were ozonation (Kharel et al., 2022; Zimmermann et al., 2012), photocatalytic treatment (Antonopoulou et al., 2016a, Antonopoulou, Konstantinou 2016b; Cobo-Golpe et al., 2022; Kazemi et al., 2023; Moustafa et al., 2020), Fenton and Fenton-like treatments (Benkayba et al., 2023; Haciane et al., 2023; Monteil et al., 2020), electrochemical oxidation (Eversloh et al., 2015), and high energy γ− or electron beam irradiations (Ghazouani et al., 2022; Jang et al., 2024). These studies have mainly focused on removal efficiency, mineralization, toxicity evolution, and transformation-product identification. Reported degradation pathways include hydroxylation, demethylation, *N*-oxidation and, depending on the treatment system, the formation of further oxidized intermediates.

From these techniques, high-energy ionizing irradiation is an important advanced treatment approach in water purification. In radiation-induced water treatment, two main irradiation modalities are commonly distinguished: gamma irradiation and electron beam treatment. Although both methods rely on the same fundamental radiation chemistry of water, they differ in dose rate, penetration depth, operation mode, and technological implementation. The electron beam water treatment is an emerging technology, which, besides ozonation, is used in large scale industrial applications. Nowadays, the industry applies facilities that can treat 10,000 – 30,000 m^3 wastewater daily IAEA, 2007, 2020). The technology does not need additives, the reactions does not depend on the turbidity, the water to be treated continuously flows under the electron accelerator window (reaction time is 1 – 2 s) and compared to gamma irradiations, when the accelerator is switched off, there is no radiation hazard. Once the purification system is established the

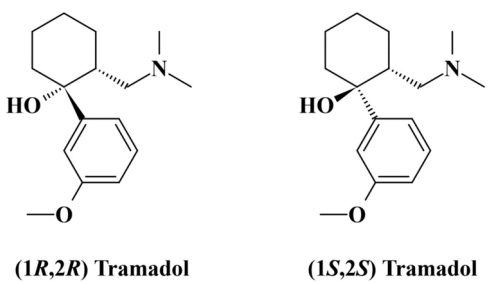

Fig. 1. Structural formula of Tramadol.

price of treatment is much smaller than with other technologies (~ 0.2 USD m^{-3}) (IAEA, 2007, 2020; Rózsa et al., 2019).

In addition to its demonstrated effectiveness in the removal of various environmental pollutants, high-energy ionizing radiation (electron beam, γ-rays) offers a highly suitable and well-controlled experimental approach for mechanistic investigations. In dilute aqueous solution the energy of ionizing particles is overwhelmingly absorbed by water and the chemical changes in the solute molecules occur through the emergence of reactive intermediates of water radiolysis. These reactive species are: hydroxyl radical ($^{\bullet}OH$, 0.28), hydrated electron (e^-_{aq}, 0.28) and hydrogen atom ($H^{\bullet}$, 0.06) (Buxton, 2004, 2008). The numbers in brackets refer to the radiation chemical yields (*G*-values), in μmol J^{-1} units. Under practical conditions, when water is air-saturated, the dissolved O_2 eliminates e^-_{aq} and $H^{\bullet}$ transforming them into less reactive superoxide radical anion/perhydroxyl radical pair ($O_2^{\bullet-}/HO_2^{\bullet}$) (p$K_a$ 4.8, Bielski et al., 1985). In N_2O saturated solutions e^-_{aq} converts to $^{\bullet}OH$ (Janata and Schuler, 1982). Whereupon, in air and N_2O saturated solutions, practically only $^{\bullet}OH$ takes part in solute degradation. For the study of e^-_{aq} reactions selectively, the usual practice is to add a few % of *tert*-butanol for removal of $^{\bullet}OH$, and to saturate the solution with N_2 to eliminate dissolved O_2.

In one of the previous works using radiolytic reactions, the authors, Ghazouani et al. (2022), focused on evaluating a combined gamma irradiation—nanofiltration treatment for TRA removal in synthetic wastewater matrix. In the other work, Jang et al. (2024) investigated TRA degradation in pure water and in several wastewater effluents, identifying degradation products and assessing the toxicity of the resulting transformation products. They reported that hydroxylation and ring cleavage are characteristic reactions for decomposition of TRA through gamma-irradiation. However, these earlier studies mainly provide product-based and performance-based information and do not directly resolve the elementary radical steps governing the earliest stages of TRA degradation. The transient kinetics techniques like pulse radiolysis fill up the gap between the reaction inducing radicals and the final (stable) products by identifying the short lived reactive (mostly radical) intermediates. In this way a much clearer picture can be obtained about the reaction paths and reaction rates.

This work combines two complementary methodological approaches: (*i*) study of free radical reactions by using pulse radiolysis, and (*ii*) characterization of removal efficiency in γ-irradiated solutions by applying such usual water analytical indicators as Chemical Oxygen Demand (COD), Total Organic Carbon (TOC) content, Biochemical Oxygen Demand (BOD) and toxicity (*Vibrio Fischeri*). This combined strategy allows us to clarify the primary radical-induced degradation steps of TRA and to relate these early-stage processes to the final radiolytic outcomes observed in pure water (PW), tap water (TW), synthetic wastewater (SWW), and purified wastewater (PWW) matrices.

2. Experimental methods

2.1. Materials

TRA was obtained from Reanal (Budapest, Hungary). The analytical grade (>98%) reagents used, for the COD, TOC and BOD measurements, were obtained from Molar Chemicals Ltd. (Halásztelek, Hungary). N_2O was provided by Messer (Budapest, Hungary). Buffer solutions were prepared using K_2HPO_4 and KH_2PO_4 purchased from Merck (Darmstadt, Germany). The redox indicators like potassium ferricyanide ($K_3Fe(CN)_6$), methyl viologen dichloride hydrate (MV^{2+}), 2,2'-azino-bis(3-ethylbenzothiazoline−6-sulfonic acid) diammonium salt (ABTS) and hydroquinone (H_2Q) were provided by Sigma-Aldrich (St. Louis, MO).

2.2. Matrices

In order to systematically investigate matrix effects on TRA degradation, experiments were carried out in pure water (PW), tap water (TW), synthetic wastewater (SWW) and purified wastewater (PWW) matrices. PW with conductivity of 0.055 μS cm^{-1} was produced by an Adrona B30 system (Adrona SIA, Riga, Latvia). TW collected directly from the local municipal drinking water supply had relatively high Inorganic Carbon (IC) content. SWW had in 1 dm^3 7 mg $(NH_4)_2SO_4$, 7 mg K_2HPO_4, 7 mg humic acid, 0.7 mg $MgSO_4$ and 81 mg $NaHCO_3$ (Reanal, Budapest, Hungary). PWW was provided by the South-Pest Wastewater Treatment Plant (SP WWTP, Budapest Sewage Works Pte Ltd., Budapest, Hungary). Their main physicochemical characteristics are summarized in Table S1.

2.3. Irradiation

Most experiments were carried out in 0.1 mmol dm^{-3} TRA solution at room temperature.

In final products experiments we used the panoramic ^{60}Co-γ irradiation facility of the Institute of Isotopes Co Ltd. (Budapest, Hungary). The dose rate of 2 kGy h^{-1} (1 Gy = 1 J kg^{-1}) was measured by ethanol-chlorobenzene dosimetry (ISO/ASTM 51538 2007). Separate sample vessels were prepared for each absorbed dose and removed from the irradiation chamber after reaching the target dose. The experiments were carried out at absorbed doses of 0, 0.4, 0.8, 1, 2.5 and 5 kGy in aerated solutions applying gentle air bubbling during irradiation in order to ensure an adequate level of dissolved oxygen.

In pulse radiolysis experiments the reactions were initiated by 800 ns pulses of 4 MeV energy electrons, the absorbed dose/pulse values in 1 cm optical cells were ~20 Gy/pulse (Földiák et al., 1988). The dose/pulse values were measured by the standard KSCN dosimetry with an $\varepsilon_{480\,nm}$ of 7850 mol^{-1} dm^3 cm^{-1} for the formed $(SCN)_2^{\bullet-}$ (Buxton and Stuart, 1995). In our experiments, $^{\bullet}OH$ reactions were investigated in N_2O-saturated (0.025 mol dm^{-3}) solutions, where hydrated electrons were converted into additional $^{\bullet}OH$ radicals, making this system a particularly clean and well-defined source of $^{\bullet}OH$ (Wojnárovits and Takács, 2013). The solution was continuously bubbled during the measurements and for 30 min prior to the experiment to ensure complete saturation of the 0.5 dm^{-3} solution. For the experiments performed at different pH values, the pH was adjusted to the desired value using NaOH and perchloric

acid.

Redox indicators were applied in the pulse radiolysis experiments to obtain complementary mechanistic information on the transient species formed during TRA degradation. These compounds help to distinguish between oxidizing and reducing intermediates and thereby support the interpretation of the observed transient absorption spectra. To facilitate readability, the specific reactions of ferricyanide, MV^{2+}, ABTS and H_2Q are described in detail in the Results and Discussion section, where they are directly related to the experimental observations. In these experiments first we prepared the TRA containing solutions, which eventually contained also the additives, and then poured the solutions into the bubbler. The bubbler was connected with the optical cell and the solution flowed through the optical cell during the whole experiment.

2.4. Analytical techniques

The details of our experimental methods were described in previous publications (Kovács et al., 2020, 2022, 2023); here we briefly repeat some of the procedures used. The organic matter content of the irradiated samples was characterized using standard water analysis parameters: COD (mg O_2 needed to oxidize organics in 1 dm^3), BOD (mg O_2 needed for biochemical oxidation in 1 dm^3), TOC (mg C in 1 dm^3) content and acute toxicity bioassay.

In COD measurements we followed the description of the ISO, (6060) (1989). The digestion of the organic impurities in the aqueous sample was carried out in sulfuric acid using dichromate for the oxidation and containing silver sulfate (Ag_2SO_4) as catalyst and mercury sulfate ($HgSO_4$) to eliminate the possible disturbing effect of the chloride ion (Cl^-). Following 2 h refluxing at 150 °C the dichromate consumption was determined by titration with ferrous ammonium sulfate ($Fe(NH_4)_2(SO_4)_2 \times 6\ H_2O$) solution in the presence of ferroin indicator (1–10-(ortho) phenanthroline monohydrate).

The TOC was measured using a Shimadzu TOC-L CSH/CSN analyser based on catalytic high-temperature combustion and non-dispersive infrared detection of the formed CO_2. Hydrochloric acid and phosphoric acid were used for sample acidification prior to analysis. Acidification converts dissolved inorganic carbon species, such as carbonate and bicarbonate ions, into carbonic acid, which decomposes to CO_2 and removed from the sample by purging.

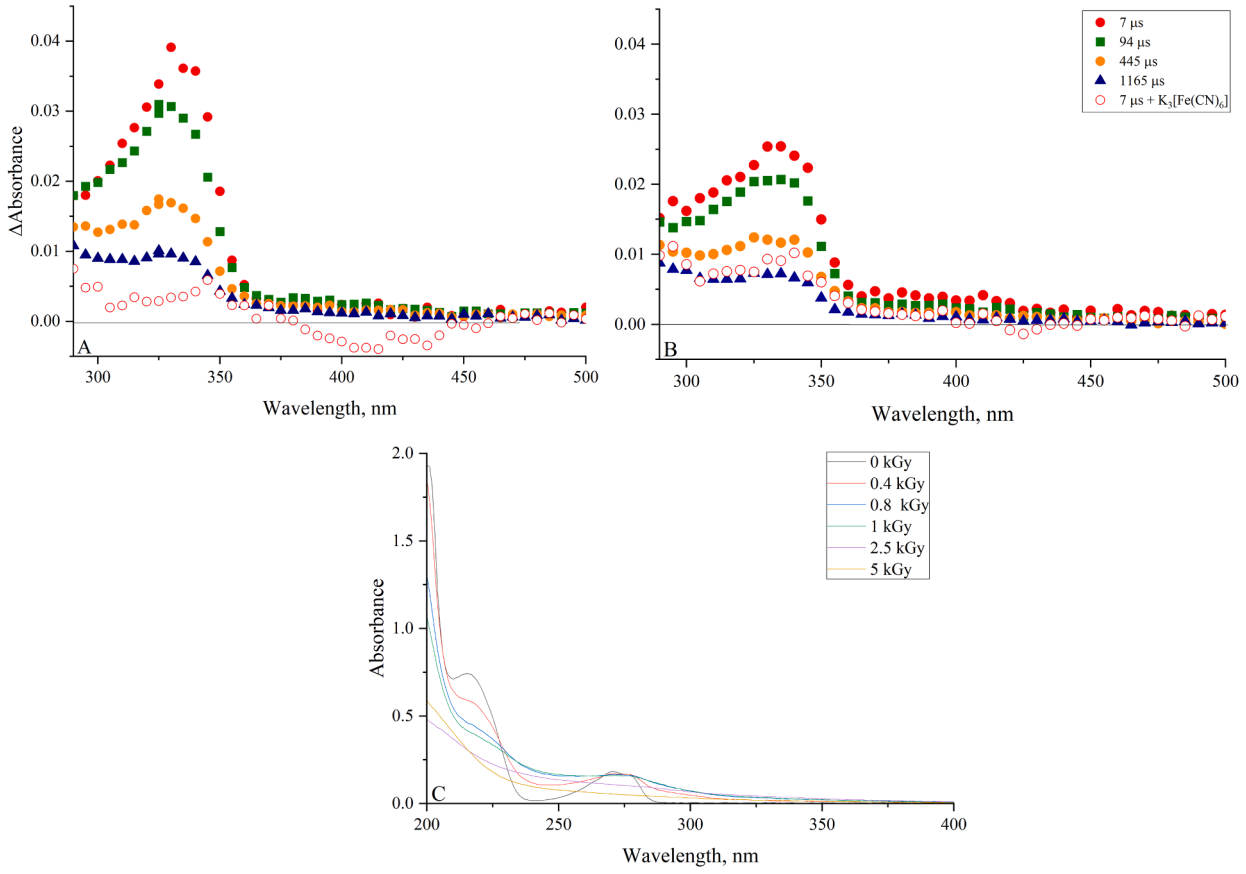

Fig. 2. Absorption spectra of the transient radical intermediates formed in the $^{\bullet}OH$ + TRA reaction at pH 7 (A) and 10.5 (B) at 7, 94, 445, and 1165 µs after the electron pulse in N_2O saturated 0.1 mmol dm^{-3} TRA solutions. Both figures show a spectrum taken in the presence of 0.1 mmol dm^{-3} $K_3Fe(CN)_6$. This additive is used to identify the hydroxycyclohexadienyl radical intermediates. (C) shows the UV-Vis absorption spectra of TRA solutions irradiated to different absorbed doses.

According to the standard 5-day incubation method, BOD was evaluated in the presence of a mixed microorganism (MN 715 filtrated inoculum from activated sludge basin, SP WWTP) population degrading the organic pollutants, the pressure change in closed bottle was used to determine the amount of O_2 consumption. The measurements were carried out in an OxiTOP® Control BOD Respirator System in compliance with the DIN EN 1899–1 (1999) Standard (DIN EN ISO, 1899–1 n.d., Wu et al., 2022). 20 cm^3 of settled activated sludge supernatant, collected from the aeration basin of the South-Pest Municipal Wastewater Treatment Plant operated by Budapest Sewage Works, Hungary, was added to 1 dm^3 of dilution water. The pH of the dilution water was adjusted to 7.2 ± 0.2 using NaOH or HCl. Allylthiourea was added as a nitrification inhibitor to ensure that oxygen consumption originated predominantly from the biodegradation of organic carbon rather than from nitrification.

For assessment of the toxic effects of TRA and its transformation products in different water matrices we carried out Microtox toxicity® bioassays. This test is based on monitoring changes in the light emission of the *Vibrio fischeri* bacteria caused by chemicals in accordance with the DIN EN ISO (1134)8–2:(1999) (1999) Standard applying 30 min incubation at 15 ± 2 °C.

In the radiolysis of aerated solutions, formation of the hydrogen peroxide (H_2O_2) may interfere the biochemical tests due to its toxic properties (Bezsenyi et al., 2021; Illés et al., 2017; Kovács et al., 2017; Sági et al., 2018; Zona and Solar, 2003). The residual H_2O_2 was eliminated using manganese dioxide (MnO_2, 5 g dm^{-3}, Sigma-Aldrich, USA) before BOD, and catalase enzyme (1 mg cm^{-3} in 50 mmol dm^{-3} phosphate buffer, Sigma-Aldrich) before Microtox® tests.

3. Results and Discussion

3.1. Free radical reactions detected by time resolved kinetic technique

3.1.1. Reactions of the hydroxyl radical

In reactions of the primary species formed, such as the strongly oxidizing and electrophilic $^{\bullet}OH$, the chemical structure of the target molecule may govern the preferred sites of attack and the ensuing reaction pathways. In $^{\bullet}OH$ reactions three probable reactive places may be distinguished in the degradation of a molecule that has aromatic and amino functions and also saturated parts like TRA: (*i*) $^{\bullet}OH$ addition to the aromatic ring *via* forming hydroxycyclohexadienyl radicals; (*ii*) the reactions involving the amino function *via* two pathways: (*a*) by *H*-atom abstraction from the *C*-atoms next to *N* developing α-aminoalkyl radicals ($R^1R^2NC^{\bullet}HR^3$) and (*b*) direct attack on the *N*-atom yielding aminium and aminyl radicals ($R^1R^2N^{\bullet+}R^3$ and $R^1R^2N^{\bullet}$); and (*iii*) *H*-abstraction from the *C*-atoms in the cyclohexane ring or from the –O–CH_3 moiety. The aromatic ring is expected to be susceptible to $^{\bullet}OH$ addition because of its relatively high electron density, which may lead to hydroxylated intermediates and, in subsequent steps, further oxidation or ring opening. In parallel, reactions involving the amino/aliphatic part of the molecule may proceed through *H*-abstraction and/or oxidation pathways, contributing to demethylation and *N*-oxidation products.

Organic radicals are often identified from the transient absorption spectra obtained in pulse radiolysis. TRA practically has no UV absorbance above 290 nm (Kucuki and Kadioglu, 2007; Zidane et al., 2019), which would disturb taking the transient spectra above this wavelength (Fig. 2 (C)). The transient spectra obtained from $^{\bullet}OH$ reactions were recorded from 290 to 500 nm wavelength at pH 7 and 10.5 in N_2O saturated pure water (PW) solutions. At both pH's the transient spectra show an absorption band with a λ_{max} of 330 nm. At pH 7 (Fig. 2 (A)) this band is more intense than the corresponding band detected at pH 10.5 (Fig. 2 (B)). The time profiles of the transient absorbances hardly differ at the two pH values: at pH 10.5 the signal decreases more rapidly, indicating different decay behavior of the transient intermediates. Assuming as a first approximation that the 330 nm absorbance is dominated by one intermediate, and the total yield of $^{\bullet}OH$ in N_2O saturated solution is 0.57 μmol J^{-1} (Janata and Schuler, 1982), the ε_{max} values can be estimated to be 3600 and 2100 mol^{-1} dm^3 cm^{-1}, respectively, at pH 7 and 10.5. The spectral characteristics of TRA at pH 7 are similar to those reported in anisole radiolysis, in both molecules a methoxy group is attached on the aromatic ring. For the anisole transient product (suggested to be hydroxycyclohexadienyl radical) Holcman, Sehested (1976) published λ_{max} = 320 nm and ε_{max} = 3400 mol^{-1} dm^3 cm^{-1}, while O'Neill et al. (1975) found λ_{max} = 320 nm and ε_{max} = 4050 mol^{-1} dm^3 cm^{-1}.

For identification of the reactive intermediates, we used four redox indicators: $Fe(CN)_6^{3-}$, MV^{2+}, ABTS and H_2Q. The absorbance characteristics together with the results obtained are given in Table S2 (Das et al., 2003; Schuler et al., 1981; Veltwisch and Asmus, 1982; Watanabe and Honda, 1982; Wolfenden and Willson, 1982; Mancini et al., 2026). Eqs. (1) – (4) illustrate the reactions of redox indicators.

$$HOC_6H_6^{\bullet} + [Fe(CN)_6]^{3-} \rightarrow C_6H_5OH + [Fe(CN)_6]^{4-} + H^+ \quad (1)$$

$$R^1R^2NC^{\bullet}HR^3 + MV^{2+} \rightarrow MV^{\bullet+} + R^1R^2N^+ = CHR^3 \quad (2)$$

$$R^1R^2N^{+\bullet}R^3 + ABTS \rightarrow ABTS^{\bullet+} + R^1R^2NR^3 \quad (3)$$

$$R^1R^2N^{\bullet} + HQ^- \rightarrow Q^{\bullet-} + R^1R^2NH \quad (4)$$

$[Fe(CN_6)]^{3-}$ ions transform hydroxycyclohexadienyl radicals to stable phenol type products as we show in Eq. (1) on the example of the radical produced in $^{\bullet}OH$ addition to benzene ($HOC_6H_6^{\bullet}$) (Anderson, 1979; Madhavan and Schuler, 1980; Steenken and Neta, 1982). In the presence of $[Fe(CN)_6]^{3-}$ a great decrease was observed in the intensity of the λ_{max} = 330 nm band (Fig. 2 (A) and (B)); at the same time bleaching (negative absorption) appeared at 420 nm, at the maximum of $[Fe(CN_6)]^{3-}$ absorbance showing the reactions of intermediates with $Fe(CN)_6^{3-}$. The strong effect of the $[Fe(CN_6)]^{3-}$ on the λ_{max} = 330 nm absorbance reveals the presence of

hydroxycyclohexadienyl radicals. Using the decrease of the 330 nm absorbance and the negative absorbance at 420 nm, we calculated radical yields of 0.48 and 0.28 μmol J^{-1}, respectively, at pH 7 and 10.5. It should be mentioned that the bleaching may not be completely due to hydroxycyclohexadienyl radical reactions, since other radicals, if they form, e.g., benzyl and alkyl, in rather slow reactions may also react with $[Fe(CN_6)]^{3-}$ (Merga et al., 1996; Stefanic et al., 2001).

$^{\bullet}$OH addition to the ring may take place at any carbon atom. However, based on the analysis of ring hydroxylated products *ortho* and *para* additions are suggested to be preferred (Eversloh et al., 2015; Antonopoulou et al., 2016a). $^{\bullet}$OH addition at the *ipso* position to the methoxy group is expected to yield demethylated product, as it is suggested in the case of anisole (Li and Jenks, 2000).

As intermediates with radical sites at the *N*-atom have absorbances below 290 nm, they are invisible in our transient spectra taken in the 290 – 500 nm wavelength range. However, using the indicators shown in Table S2, their formation can be proved, the yields can be calculated. As mentioned above, $^{\bullet}$OH may react with the *H*-atoms on neighbouring *C*-atoms to the amino group (Eq. (2)). The *α*-aminoalkyl radicals ($R^1R^2NC^{\bullet}HR^3$) that form in such reactions have reducing character. These radicals reacting with MV^{2+} convert to $MV^{\bullet+}$ which exhibits maxima at 395 and 600 nm with ε_{max} of 42,000 and 13,300 mol^{-1} dm^3 cm^{-1} (Das et al., 2003; Watanabe and Honda, 1982), respectively. As Fig. 3 shows at pH 7 there are relatively weak absorption bands at 395 and 600 nm suggesting low *α*-aminoalkyl radical yield. However, at pH 10.5 strong bands appear at 395 and 600 nm. Fig. 3 Inset depicts the pH dependence of absorbance at 395 nm, measured in the presence MV^{2+}. The values strictly follow the trend of proportion/deprotonated at the amino group, showing much higher rate of *H*-abstraction from neighbouring *C*-atoms next to the amino group in the deprotonated molecule.

In the reaction of $^{\bullet}$OH with *N*-atom aminium ($R^1R^2N^{\bullet+}R^3$) and aminyl ($R^1R^2N^{\bullet}$) radicals may form. The yields of these radicals were determined using their reaction with ABTS and H_2Q (Eqs. (3) and (4)). In these reactions the forming radicals are $ABTS^{\bullet+}$ with λ_{max} of 415 nm and ε_{max} of 36,000 mol^{-1} dm^3 cm^{-1} (Wolfenden and Willson, 1982), and $Q^{\bullet-}$ with λ_{max} = 430 nm and ε_{max} = 7200 mol^{-1} dm^3 cm^{-1} (Veltwisch and Asmus, 1982), respectively. Using the measured absorbances (Figs. 4 and 5) the combined yield of aminium + aminyl radical was calculated to be 0.08 and 0.07 at pH 7 and 10.5. We mention that aminium radical formation was also proposed in the Ferrate (VI) oxidation reactions of TRA (Zimmermann et al., 2012).

The second order rate constants of $^{\bullet}$OH reaction with TRA can be measured by a direct kinetic analysis and an indirect competition method using a reference reactant. For the direct determination we used the absorbance build-up at 330 nm pH 7. The concentration dependence of the pseudo-first-order build-up rate constants supplied the second order rate constant (Fig. 6 (A)). The slope of concentration dependence (the second-order rate constant) was 6.84 (±0.03) × 10^9 mol^{-1} dm^3 s^{-1}.

At pH 10.5, due to the smaller absorbance we determined the rate constant by using competition kinetics with SCN^- ions (Fig. 6 (B)), with this technique we repeated also the pH 7 measurement. SCN^- ions react with $^{\bullet}$OH with a rate constant of 1.06 × 10^{10} mol^{-1} dm^3 s^{-1} (Buxton and Stuart, 1995). $SCN^{\bullet}$ formed in Eq. (6) transforms to $(SCN)_2^{\bullet-}$ in Eq. (7). These anions exhibit wide absorption band with maximum at 480 nm. In Eq. (8) $A^{\bullet}_{(SCN)2}$ is the maximum absorbance value measured without TRA, and $A^{\bullet}_{(SCN)2}$ is the maximum absorbance detected in the presence of TRA. These absorbances were measured at several TRA concentrations, and $k_{\bullet OH}$ was calculated from the plot according to Eq. (8).

$$^{\bullet}OH + TRA \rightarrow TRAOH^{\bullet} \quad (5)$$

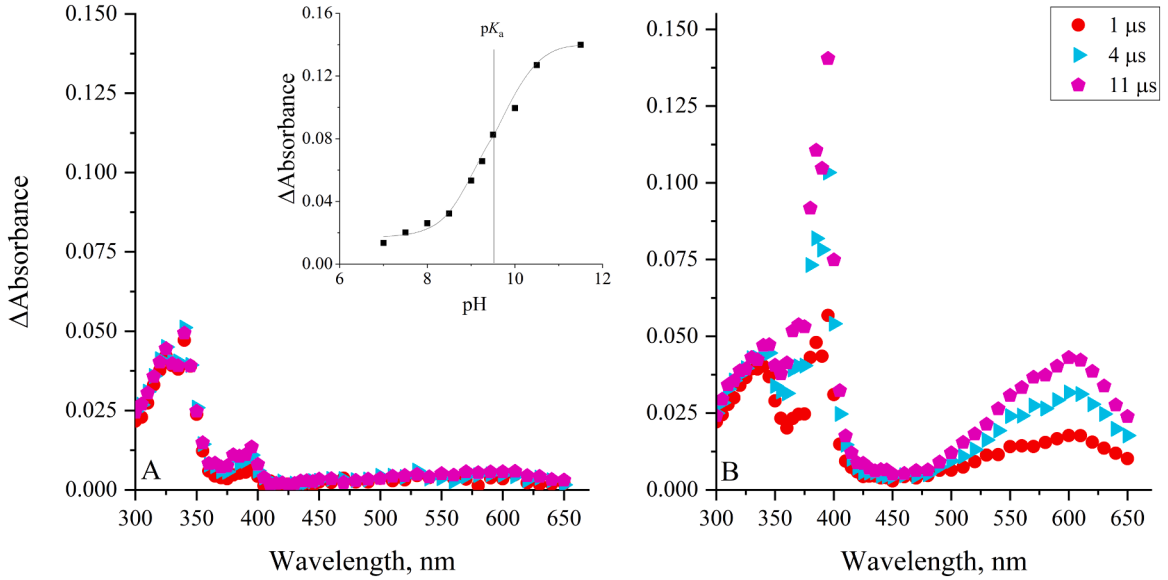

Fig. 3. Transient absorption spectra in the presence of MV^{2+} redox indicator at pH 7 (A) and 10.5 (B) in N_2O-saturated solutions; TRA and MV^{2+} concentrations were 0.4 and 0.1 mmol dm^{-3}, respectively. Inset: pH dependence of the $MV^{\bullet+}$ absorbance measured at 395 nm. The solid line was calculated using ΔAbsorbances of 0.017 and 0.14 at low and high pH, respectively, and the equilibrium constant of protonation at the *N*-atom.

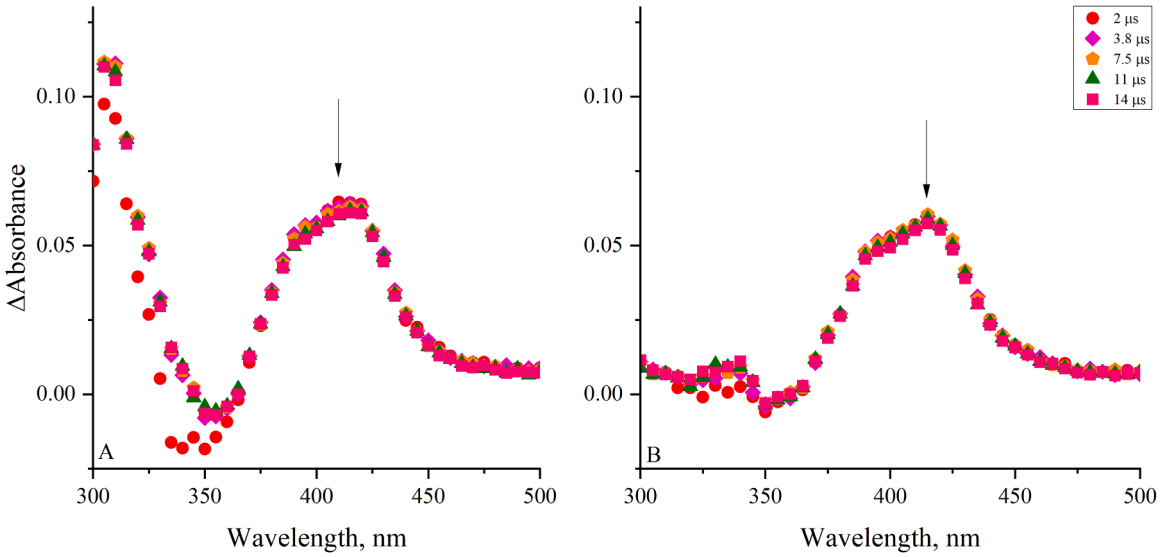

Fig. 4. Transient absorption spectra in the presence of ABTS redox indicator at pH 7 (A) and 10.5 (B) in N_2O-saturated solutions; TRA and ABTS concentrations were 0.4 and 0.07 mmol dm^{-3}, respectively.

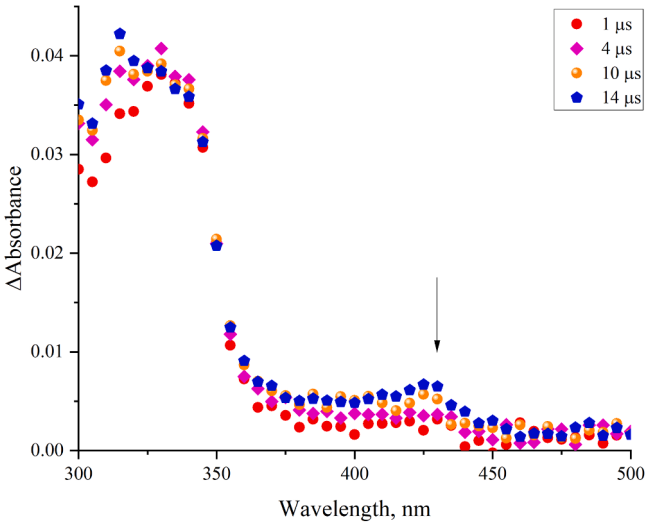

Fig. 5. Transient absorption spectra in the presence of H_2Q redox indicator at pH 7 in N_2O-saturated solutions; TRA and H_2Q concentrations were 0.4 and 0.07 mmol dm^{-3}, respectively.

$$^{\bullet}OH + SCN^{-} \rightarrow OH^{-} + SCN^{\bullet} \quad k_{\bullet OH} = 1.06 \times 10^{10} mol^{-1}\ dm^{3} s^{-1} \tag{6}$$

$$SCN^{\bullet} + SCN^{-} \rightarrow (SCN)_2^{\bullet -} \tag{7}$$

$$\frac{1}{A_{(SCN)2\bullet -}} = \frac{1}{A_{(SCN)2\bullet -,\ 0}} + \frac{1}{A_{(SCN)2\bullet -,\ 0}} \frac{k_{\bullet OH}}{k_{SCN-}} \frac{[TRA]}{[SCN^{-}]} \tag{8}$$

The rate constants at pH 7.0 and 10.5, corresponding to the protonated and non-protonated form of TRA, were found to be 6.24 (±0.62) × 10^9 mol^{-1} dm^3 s^{-1} and 8.11(±0.81) × 10^9 mol^{-1} dm^3 s^{-1}. Our values are in good agreement with literature data, namely 6.3 (±0.2) × 10^9 mol^{-1} dm^3 s^{-1} reported by Zimmermann et al. (2012) at pH 8 and 5.59 (±0.03) × 10^9 mol^{-1} dm^3 s^{-1} reported by Monteil et al. (2020) at pH 3. Taken all together, we may get a comprehensive picture about the change of the rate constants at a broad pH range (3 — 10.5). Based on the rate constants, it can be inferred that deprotonation of the amino group increases the $^{\bullet}OH$ reactivity towards TRA. These finding is consistent with previous AOP studies on tramadol, in which the oxidation pathway and reaction kinetics were shown to be strongly influenced by the molecular structure and protonation state of the amine moiety (Zimmermann et al., 2012).

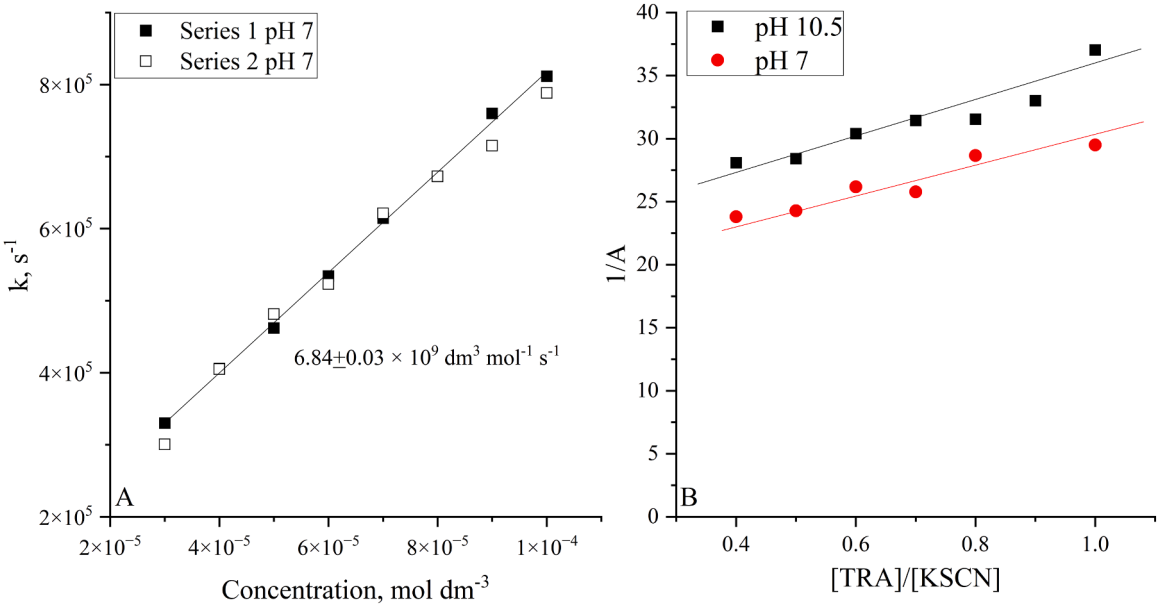

Fig. 6. (A) Concentration dependence of the pseudo-first-order rate constants of absorbance build-up in N_2O saturated solution at pH 7. (B) Determination of the rate constant of $^{\bullet}OH$ + TRA reaction at pH 7 and 10.5 by the competitive method.

Similar pH-dependent trends have been reported by Simić et al. (1971) for a series of aliphatic amines, where rate constants up to ~3 × 10⁸ mol⁻¹ dm³ s⁻¹ were found for protonated species and up to ~1 × 10¹⁰ mol⁻¹ dm³ s⁻¹ for the non-protonated ones. In agreement with these results, Karroum et al. (2024) based on UV/persulfate experiments established that the non-protonated TRA decomposes faster than the protonated one.

The differences in the transient absorption spectra taken at low and high pH (Fig. 2) indicate that the relative contribution of competing pathways changes with pH. In particular, the lower absorbance at 330 nm at high pH may reflect a redistribution of transient radical intermediates rather than a decrease in the overall reactivity of the system. This interpretation is consistent with an increased contribution of reactions involving the amino functionality at high pH, in addition to $^{\bullet}OH$ addition to the aromatic ring. The analogy with the results of Simić et al. (1971) and the spectra obtained in the presence of MV^{2+} clearly indicate that this additional reaction produces *α*-aminoalkyl radical. In protonated form there is no lone pair available for the reactant, which can, e.g., stabilize the *α*-aminoalkyl radical formed by *H*-atom elimination from a neighbouring *C*-atom, next to *N* (Simić et al., 1971; Szabó et al., 2017). The yield of these radicals at low pH is low, 0.02 μmol J^{-1}, the yield increases as the fraction of the non-protonated form at the *N*-centre increases (Fig. 3). Well above the pK_a it is 0.2 μmol J^{-1}. The yield of the nitrogen centred aminium + amininyl radicals at low pH and high pH is 0.08 and 0.07 μmol J^{-1}. The estimated summarized yields of cyclohexadienyl, α-aminoalkyl, aminium and aminyl radicals, 0.577 and 0.55 μmol J^{-1}, practically agree with the $^{\bullet}OH$ yield of 0.57 μmol J^{-1}, suggesting low yields for the alkyl radical productions at the cyclohexane ring or at the methoxy group. Albeit *H*-elimination from the methoxy group, based on the example of anisole, may also contribute to demethylated product formation (Li and Jenks, 2000).

As we showed there are important differences in the distribution of organic radical intermediates formed in $^{\bullet}OH$ reactions at low pH and high pH. These differences are expected to lead to different degradation rates and products.

3.1.2. *Reaction of the hydrated electron*

The experiments were carried out in N_2 bubbled solution for deoxygenation and contained 5 vol% *tert*-butanol to remove $^{\bullet}OH$ from the system (Eq. (9)). The transient spectrum (not shown) obtained in hydrated electron reaction, actually shows the absorption spectrum of e^-_{aq} (Buxton, 2004, 2008). The rate constant of reaction was measured following the decay of e^-_{aq} absorbance at 600 nm (not shown); it was found to be 3.15 (±0.26) × 10^9 mol^{-1} dm^3 s^{-1}.

$$OH^{\bullet} + (CH_3)_3COH \rightarrow H_2O + HOC(CH_3)_2CH_2^{\bullet} \quad (9)$$

Owing to the low rate constant of the e^-_{aq} + TRA reaction, together with the high rate constant of e^-_{aq} reaction with dissolved oxygen (1.9 × 10^{10} mol^{-1} dm^3 s^{-1}) and the high O_2 concentration under the practical conditions (0.25 mmol dm^{-3}), e^-_{aq} reactions do not contribute significantly to degradation of TRA.

3.2. *Degradation of TRA: Dose-Response of water quality indicators*

Water quality indicators like COD, TOC, BOD_5 and toxicity give an extensive understanding about oxidation and mineralization processes and removal efficiency. An index combining from COD and TOC, Average Oxidation State (AOS) is also often used to

characterize the progress of oxidation: AOS = 4 × ((TOC – COD)/TOC) (COD and TOC are expressed in mmol dm^{-3} O_2 and C, respectively) (Giannakis et al., 2015). AOS, according to the definition, changes between −4 for CH_4 and + 4 for CO_2. Based on the BOD_5/COD ratio, the starting molecule and its transformation products may be assessed regarding their biodegradability: it provides insight into the kinetics of biodegradation. Toxicity measurements using the marine bacterium *Vibrio fischeri* as test organism give information about the harmful effects of organic matters.

3.2.1. Pure water (PW)

To obtain a clear picture of the fundamental reaction pathways without the interfering matrix components, as a first step, the degradation was investigated in PW. In aqueous solutions TRA has the characteristic aromatic UV absorption band with peaks at 271 and 276 nm (Fig. 2 (C)) (Kucuki and Kadioglu, 2007). The spectra taken on the non-irradiated and irradiated samples indicate that at c. a. 1 kGy dose the intact molecules practically entirely disappear from the solution and mainly the degradation products are present. Ghazouani et al. (2022) reported ~80% of degradation efficiency of pristine TRA molecules at 1 kGy absorbed dose in synthetic wastewater.

Upon γ-irradiation both COD and TOC decrease, and these changes are observed even at the lowest doses used. While the COD decrease clearly indicates oxidation, the smaller TOC decrease shows that mineralization is also initiated but remains limited (Fig. 7 (A) and (B)). Limited mineralization was also found γ-radiolysis in the experiments of Ghazouani et al. (2022).

The slope values of initial decreases were ΔCOD/Dose = 15.5 mg O_2 dm^{-3} kGy^{-1} and ΔTOC/Dose = 1.4 mg C dm^{-3} kGy^{-1}. These values are much higher than those measured e.g., for sulphonamide antibiotics: ΔCOD/Dose = 6.1 mg O_2 dm^{-3} kGy^{-1} and ΔTOC/Dose = 0.60 mg C dm^{-3} kGy^{-1} (Wojnárovits et al., 2024). The high values indicate fast TRA degradation in $^{\bullet}OH$ initiated reactions. The percentage decrease in COD is higher than in TOC: the transformation of the target molecule into partly oxidized products may occur in several steps, mineralization into CO_2 and H_2O requires more oxidants and multiple successive reactions.

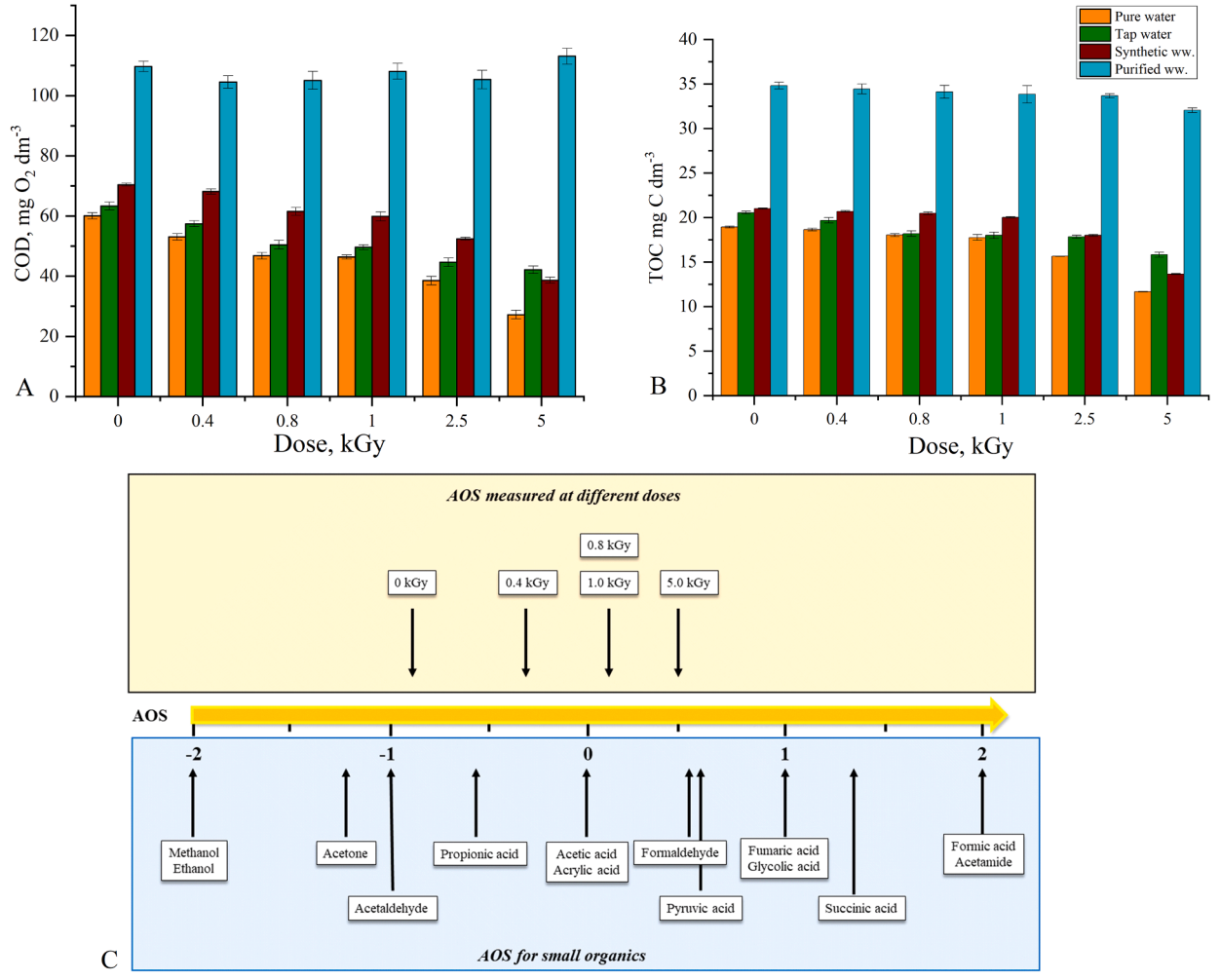

Fig. 7. Dose dependence of the COD (A) and TOC (B) values in different aqueous matrices of 0.1 mmol dm^{-3} TRA; AOS values determined at different doses (arrows above AOS line) and AOS values calculated for a few small organic molecules (arrows below the line) (C).

AOS value for TRA solution was measured to be −0.78 (theoretical value −1.12). AOS increased with the absorbed dose to the positive range above 0.8 kGy, i.e., increased to the range where strongly oxidized fragments, mostly acids, dominate the product spectrum. In Fig. 7 (C) we show calculated AOS values for a large number of small organic molecules. In the electro-Fenton experiments of Monteil et al. (2020), where also •OH was the main initiating radical, oxalic-, glycolic- and fumaric acids were identified as highly oxidized fragments. The AOS values of these compounds are 3, 1 and 1, respectively. In our experiments, formation of organic acid fragments is also supported by the strong decrease of pH: the initial pH 6.03 decreased to 4.28 at 1 kGy and to 3.76 at 5 kGy absorbed dose (Fig. 8, Inset).

Together with the decrease of COD the BOD_5/COD ratio increases. According to commonly applied criteria this ratio allows the treated samples to classify with respect to their biodegradability as non-biodegradable, slowly biodegradable, biodegradable and easily biodegradable groups (Abbas et al., 2022; Metcalf and Eddy, 2003). 0.1 mmol dm^{-3} TRA solution with BOD_5/COD of 0.16 is non-biodegradable (Fig. 9). After irradiation at 1 kGy the ratio is above 0.4, fulfilling the minimum requirement for biodegradation. Increasing the absorbed dose there is a further increase in the ratio and the remaining, partly oxidized organic content becomes easily biodegradable at 2.5 kGy dose.

In addition to biodegradability, an equally important aspect of biological evaluation is the ecotoxicity of both the parent compound and its transformation products. In these measurements TRA at 0.1 mmol dm^{-3} concentration in PW was found to be non-toxic indicated by the absence of fluorescence inhibition (Fig. 8). Similar results are published in the literature (Antonopoulou et al., 2020; Nikitin et al., 2022; Patel et al., 2019; Subedi et al., 2019). The fluorescence inhibition increased in the initial period of treatment, at 0.8 kGy absorbed dose it went up to 17%, and with the increase of dose vanished, at 5 kGy dose no fluorescence inhibition was detected. The increase indicates that some of the first formed products are slightly toxic. This dose dependence reveals the importance of selection the optimal dose.

Several studies have addressed the question of why the overall toxic effect may be observed higher during the transformation of TRA (Antonopoulou et al., 2020; Patel et al., 2019). This temporary increase is often attributed to the formation and co-occurrence of transformation products. The major degradation products (*N*-desmethyltramadol (*N*-DES-TRA) and tramadol *N*-oxide (*N*-OX-TRA) were reported to cause higher bioluminescence inhibition than TRA.

3.2.2. Matrix effect on the removal efficiency, degradation in tap water (TW), synthetic wastewater (SWW) and purified wastewater (PWW) matrices

The dissolved constituents in TW, SWW and PWW matrices strongly influence the degradation by controlling the availability of reactive species. The matrix effect is often quantified in terms of the radical scavenging capacity (Eq. (10)):

$$k'_{scav} = \sum_i k_i \quad [i] \tag{10}$$

where the *i* species (e.g., HCO_3^-/CO_3^{2-}, Cl^-, NO_2^- etc.) compete with •OH. Because the investigated matrices differed in their COD, TOC and IC levels, the overall scavenging capacity varied accordingly, leading to matrix-dependent differences in removal efficiency.

The experiments carried out applying the usual water analytical techniques (COD, TOC, BOD_5 and BOD_5/COD ratio) clearly indicate the efficiency of ionizing radiation treatment in TRA degradation. The COD values in the absence of TRA were 2.8, 8.1 and 68 mg O_2 dm^{-3} for TW, SWW and PWW, respectively, reflecting markedly different background organic matter contents. In the

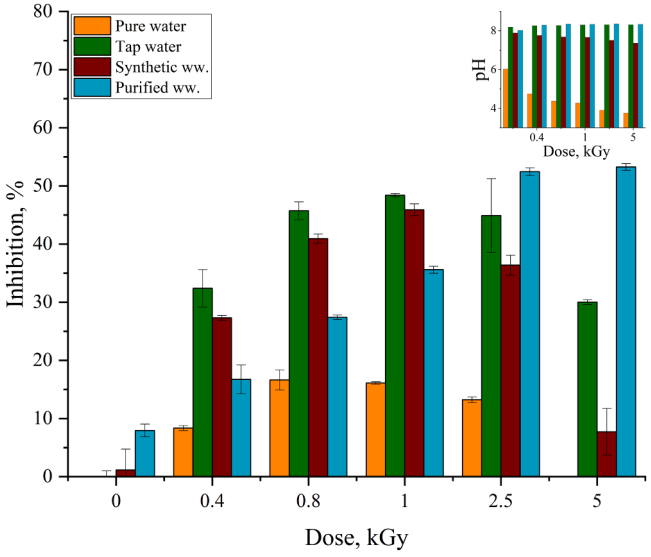

Fig. 8. Dose dependence of fluorescence inhibition in solutions containing 0.1 mmol dm^{-3} TRA, irradiated in the 0 – 5 kGy dose range. Inset: the pH values of solutions measured after irradiation with different doses in different matrices.

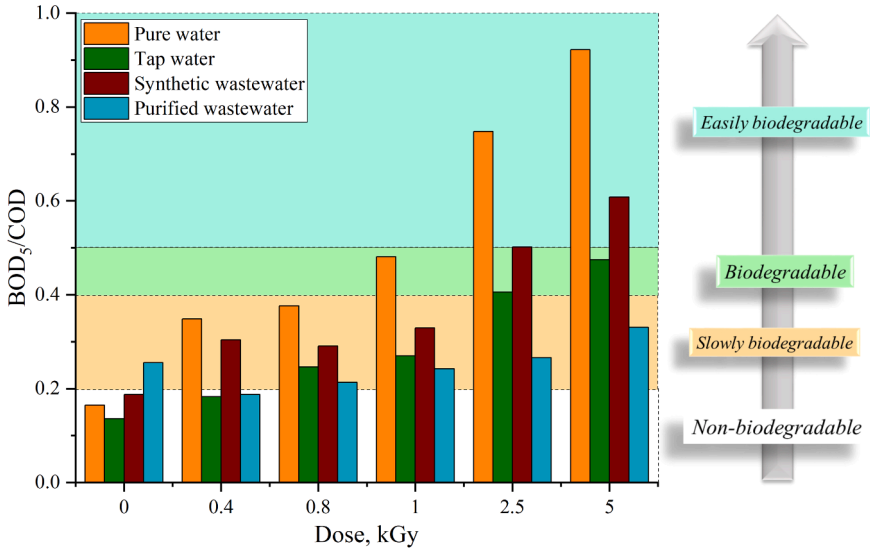

Fig. 9. Effect of absorbed dose on the BOD_5/COD ratio in various matrices of 0.1 mmol dm^{-3} TRA. In the figure we show the degradability limits taken from the works of Abbas et al. (2022) and Metcalf and Eddy (2003).

irradiated TW and SWW solutions both COD and TOC decreased with the absorbed dose (Fig. 7). However, this decrease was smaller than in pure water matrix. In TW, SWW and PWW matrices the pH was around 8 and practically did not change during the irradiation. Presumably, the dissolved material present in samples exerted some buffering effect. In the dielectric barrier discharge experiments of Babalola et al. (2023) also no pH change was found. They attributed this observation to the buffering properties of carbonate ions, present in wastewater. The original PWW matrix had high organic content, in TRA solution hardly any decrease was observed in the COD and TOC until the highest dose (Figs. 7, 5 kGy). The biodegradability, revealed by the BOD_5/COD ratios, increased with dose, at 5 kGy the organic content in all solutions, except in PWW, became biodegradable. With further increase of dose the biodegradability was also achieved in PWW (not shown). In TW and SWW the dose dependence of the fluorescence inhibition was similar to that observed in PW matrix, although the initial increase upon irradiation was higher. In PWW considerable fluorescence inhibition, 20%, was measured even in the non-irradiated solution. The percentage inhibition increased continuously during the irradiation. A decrease is expected at doses higher than 5 kGy as further oxidation/mineralization proceeds.

The predominant inorganic and organic matters in the investigated matrices include CO_3^{2-}, HCO_3^-, CO_3^{2-}, NO_2^-, Cl^-, Fe^{2+} and humic acid. These impurities, by acting as radical scavengers, strongly retard the degradation of the target compound. Based on the bimolecular rate constants, the strongest inhibitory effect can be attributed to nitrite and chloride ions (Fig. 10, Barr et al., 2024; Goldstone et al., 2002; Jaysons et al., 1973; Leresche et al., 2021; Wojnárovits et al., 2020). In PWW, the background dissolved organic matter, reflected by elevated TOC and COD levels, is expected to dominate $^{\bullet}OH$ consumption and thus to markedly suppress the removal rates within the same absorbed dose window.

4. Conclusion

In this study, the pathways and kinetics of TRA reaction with the primary reactive species formed in water radiolysis were elucidated by pulse radiolysis and complemented by γ-irradiation experiments in various aqueous matrices. Pulse radiolysis revealed that $^{\bullet}OH$-initiated degradation of TRA proceeds mainly *via* aromatic addition and, at higher pH, increasingly through α-aminoalkyl radical formation, due to deprotonation of the amino group. γ-Irradiation in ultrapure water resulted in rapid parent-compound loss reflected by the decreasing COD and TOC, increasing biodegradability and a transient toxicity increase followed by detoxification at higher doses. In TW, SWW and especially PWW, the efficiency was lower due to matrix-specific radical scavenging; nitrite, chloride and dissolved organic matter are suggested to be the main inhibitors. Therefore, the mechanistic and kinetic information obtained in this work is relevant not only for understanding tramadol degradation pathways, but also for the practical development of radiation-based and other $^{\bullet}OH$-driven AOPs, where matrix composition, scavenging effects, and dose requirements must be taken into account.

Funding

This research was supported by the János Bolyai Research Scholarship of the Hungarian Academy of Sciences and by the Ministry of Culture and Innovation of Hungary from the National Research, Development and Innovation Fund financed under the OTKA FK 23 funding scheme (Project No. 146883).

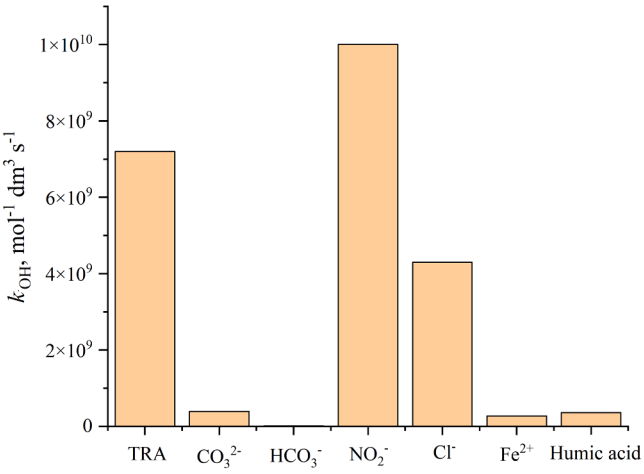

Fig. 10. The bimolecular rate constants of •OH with TRA and a few matrix constituents.

CRediT authorship contribution statement

Krisztina Kovács: Writing – review & editing, Writing – original draft, Investigation, Conceptualization. **Anna Tegze:** Investigation. **Anikó Bezsenyi:** Methodology, Investigation. **László Wojnárovits:** Writing – review & editing, Writing – original draft, Supervision, Conceptualization.

Declaration of Competing Interest

The authors declare that they have no known competing financial interests or personal relationships that could have appeared to influence the work reported in this paper.

Appendix A. Supporting information

Supplementary data associated with this article can be found in the online version at doi:10.1016/j.eti.2026.105039.

Data availability

Data will be made available on request.

References

Abbas, A.A., Yousif, Y.T., Almutter, H.H., 2022. Evaluation of Al-Thagher wastewater treatment plant. Period. Polytech. Civ. Eng. 66, 112–126. https://doi.org/10.3311/PPci.18513.

Anderson, R.F., 1979. Oxidation of the cyclohexadienyl radical by metal ions: a pulse radiolysis study. Radiat. Phys. Chem. 13, 155–157. https://doi.org/10.1016/0146-5724(79)90039-6.

Antonopoulou, M., Konstantinou, I., 2016b. Photocatalytic degradation and mineralization of tramadol pharmaceutical in aqueous TiO_2 suspensions: Evaluation of kinetics, mechanisms and ecotoxicity. Appl. Catal. A 515, 136–143. https://doi.org/10.1016/j.apcata.2016.02.005.

Antonopoulou, M., Thoma, A., Konstantinou, F., Vlastos, D., Hela, D., 2020. Assessing the human risk and the environmental fate of pharmaceutical Tramadol. Sci. Total. Environ. 710, 135396. https://doi.org/10.1016/j.scitotenv.2019.135396.

Antonopoulou, M., Hela, D., Konstantinou, I., 2016a. Photocatalytic degradation kinetics, mechanism and ecotoxicity assessment of tramadol metabolites in aqueous TiO_2 suspensions. Sci. Total. Environ. 545–546, 476–485. https://doi.org/10.1016/j.scitotenv.2015.12.088.

Ardakani, Y.H., Rouini, M.-R., 2007. Pharmacokinetics of Tramadol and its three main metabolites in healthy male and female volunteers. Biopharm. Drug. Dispos. 28, 527–534. https://doi.org/10.1002/bdd.584.

Babalola, S.O., Daramola, M.O., Iwarere, S.A., 2023. An investigation on the removal of tramadol analgesic in deionized water and final wastewater effluent using a novel continuous flow dielectric barrier discharge reactor. J. Water Proc. Eng. 56, 104294. https://doi.org/10.1016/j.jwpe.2023.104294.

Barr, L., Conrad, J.K., McGregor, C., Perron, R., Yakabuskie, P.A., Stuart, C.R., 2024. Kinetics of the reaction of ferrous ions with hydroxyl radicals in the temperature range 25−300 °C. Phys. Chem. Chem. Phys. 26, 4278–4283. https://doi.org/10.1039/D3CP03819J.

Benkayba, W., El Karbane, M., El Kacemi, K., Arhoutane, M.R., Karrouchi, K., Guessous, A., 2023. Study of tramadol removal from water by the electro-Fenton process coupled with biological post-treatment: kinetics and energetic evaluation. Int. J. Environ. Anal. Chem. 104 (20), 9260–9274. https://doi.org/10.1080/03067319.2023.2228706.

Bezsenyi, A., Sági, Gy, Makó, M., Wojnárovits, L., Takács, E., 2021. The effect of hydrogen peroxide on the biochemical oxygen demand (BOD) values measured during ionizing radiation treatment of wastewater. Radiat. Phys. Chem. 189, 109773. https://doi.org/10.1016/j.radphyschem.2021.109773.

Bielski, B.H.J., Cabelli, D.E., Arudi, R.L., Ross, A.B., 1985. Reactivity of $O_2^{\bullet-}$/$HO_2^{\bullet}$. Radic. aqueous Solut. J. Phys. Chem. Ref. Data 14, 1041–1100. https://doi.org/10.1063/1.555739.

Buxton, G.V., 2004. The radiation chemistry of liquid water: principles and applications. In: Mozumder, A., Hatano, Y. (Eds.), Charged Particle and Photon Interactions with Matter. Marcel Dekker, New York.
Buxton, G.V., 2008. An overview of the radiation chemistry of liquids. In: Spotheim-Maurizot, M., Mostafavi, M., Douki, T., Belloni, J. (Eds.), Radiation Chemistry: From Basics to Applications in Material and Life Sciences. EDP Sciences, France, pp. 3–16.
Buxton, G.V., Stuart, C.R., 1995. Re-evaluation of the thiocyanate dosimeter for pulse radiolysis. J. Chem. Soc. Faraday Trans. 91, 279–281. https://doi.org/10.1039/FT9959100279.
Cobo-Golpe, M., Fernández-Fernández, V., Arias, T., Ramil, M., Cela, R., Rodríguez, I., 2022. Comparison of UV, chlorination, UV-hydrogen peroxide and UV-chlorine processes for tramadol removal: Kinetics study and transformation products identification. J. Environ. Chem. Eng. 10, 107854. https://doi.org/10.1016/j.jece.2022.107854.
Council Directive 91/271/EEC. ⟨https://eur-lex.europa.eu/eli/dir/1991/271/oj⟩ (accessed 01 June 2026).(n.d.).
Das, Z.N., Ghanty, T.K., Pal, H., 2003. Reactions of methyl viologen dication (MV^{2+}) with H atoms in aqueous solution: Mechanism derived from pulse radiolysis measurements and ab initio MO calculations. J. Phys. Chem. A 107, 5998–6006. https://doi.org/10.1021/jp022614r.
DIN EN ISO 11348-2:1999, 1999. Determination of the Inhibitory Effect of Water Samples on the Light Emission of Vibrio Fischeri (Luminescent Bacteria Test) Part 2: Method Using Liquid-Dried Bacteria.
DIN EN ISO 1899-1 Determination of biochemical oxygen demand after n days (BODn) - Part 1: Dilution and seeding method with allylthiourea addition (ISO 5815: 1989, modified)(n.d.).
Directive 2000/60/EC. ⟨https://eur-lex.europa.eu/eli/dir/2000/60/oj⟩ (accessed 01 June 2026).(n.d.).
Eversloh, C.L., Schulz, M., Wagner, M., Ternes, T.A., 2015. Electrochemical oxidation of tramadol in low-salinity reverse osmosis concentrates using boron-doped diamond anodes. Water Res. 72, 295–304. https://doi.org/10.1016/j.watres.2014.12.021.
Földiák, G., Hargittai, P., Kaszanyiczki, Wojnárovits, L., 1988. A computer controlled pulse radiolysis laboratory. J. Radioanal. Nucl. Chem. Artic. 125, 19–28. https://doi.org/10.1007/bf02041745.
Ghazouani, S., Boujelbane, F., Ennigrou, D.J., Van der Bruggen, B., Mzoughi, N., 2022. Removal of tramadol hydrochloride, an emerging pollutant, from aqueous solution using gamma irradiation combined by nanofiltration. Process. Saf. Environ. Prot. 159, 442–451. https://doi.org/10.1016/j.psep.2022.01.005.
Giannakis, S., Gamarra Vives, F.A., Grandjean, D., Magnet, A., De Alencastro, L.F., Pulgarin, C., 2015. Effect of advanced oxidation processes on the micropollutants and the effluent organic matter contained in municipal wastewater previously treated by three different secondary methods. Water Res. 84, 295–306. https://doi.org/10.1016/j.watres.2015.07.030.
Goldstone, J.V., Pullin, M.J., Bertilsson, S., Voelker, B.M., 2002. Reactions of hydroxyl radical with humic substances: Bleaching, mineralization, and production of bioavailable carbon substrates. Environ. Sci. Technol. 36, 362–374. https://doi.org/10.1021/es0109646.
Haciane, Y.M., Bouafia, S.C., Chabani, M., Benramdan, I.-K., Mebtouche, M., Neffa, M., Touzani, R., 2023. Optimization and modeling of Tramadol hydrochloride degradation by the homogenous photo-Fenton-like system assisted by in situ H_2O_2 formation. Water Sci. Technol. 87, 1174–1186. https://doi.org/10.2166/wst.2023.039.
Holcman, J., Sehested, K., 1976. Anisole radical cation reactions in aqueous solution. J. Phys. Chem. 80, 1642–1644. https://doi.org/10.1021/j100555a027.
IAEA, 2007. Radiation Processing, Environmental Applications. International Atomic Energy Agency, Vienna, Austria.
IAEA 2020. The largest wastewater facility…, Available online ⟨https://www.iaea.org/newscenter/news/started-with-iaea-support-chinas-electron-beam-industry-opens-worlds-largest-wastewater-treatment-facility⟩ (accessed on 01 June 2026).
Illés, E., Tegze, A., Kovács, K., Sági, Gy, Papp, Z., Takács, E., Wojnárovits, L., 2017. Hydrogen peroxide formation during radiolysis of aerated aqueous solutions of organic molecules. Radiat. Phys. Chem. 134, 8–13. https://doi.org/10.1016/j.radphyschem.2016.12.023.
ISO 6060, 1989. International Standard, Water-quality: Determination of Chemical Oxygen Demand, 2nd Edn.
ISO/ASTM 51538, 2007. Pract. Use ethanol-chlorobenzene Dosim. Syst.
Janata, E., Schuler, R.H., 1982. Rate constant for scavenging e^-_{aq} in nitrous oxide-saturated solutions. J. Phys. Chem. 86, 2078–2084. https://doi.org/10.1021/j100208a035.
Jang, H., Kim, T.-H., Jeon, J., 2024. Degradation of micropollutants by gamma irradiation: Insight of transformation product formation explored by suspect and non-target screening using LC-HRMS. J. Environ. Chem. Eng. 12, 111659. https://doi.org/10.1016/j.jece.2023.111659.
Jayson, G.G., Parsons, B.J., Swallow, A.J., 1973. Some simple, highly reactive, inorganic chlorine derivatives in aqueous solution. Their formation using pulses of radiation and their role in the mechanism of the Fricke dosimeter. J. Chem. Soc. Faraday Trans. 1 69, 1597–1607. https://doi.org/10.1039/F19736901597.
Karroum, W.B., Baalbaki, A., Nasreddine, A., Oueidat, N., Ghauch, A., 2024. From batch system toward continuous UV/PS based AOP reactor: the case of tramadol effluent degradation. Environ. Sci. Adv. 3, 1234. https://doi.org/10.1039/D4VA00103F.
Kazemi, F., Zamani, H.A., Abedi, M.R., Ebrahimi, M., 2023. Synthesis and comparison of three photocatalysts for degrading tramadol as an analgesic and widely used drug in water samples. Environ. Res. 225, 114821. https://doi.org/10.1016/j.envres.2022.114821.
Kharel, S., Tentscher, P.R., Kai Bester, K., 2022. Further transformation of the primary ozonation products of tramadol- and venlafaxine *N*-oxide: Mechanistic and structural considerations. Sci. Total. Environ. 845, 157259. https://doi.org/10.1016/j.scitotenv.2022.157259.
Kostanjevecki, P., Petric, I., Loncar, J., Smital, T., Ahel, M., Senka Terzic, S., 2019. Aerobic biodegradation of tramadol by pre-adapted activated sludge culture: Cometabolic transformations and bacterial community changes during enrichment. Sci. Total. Environ. 687, 858–866. https://doi.org/10.1016/j.scitotenv.2019.06.118.
Kovács, K., Sági, Gy, Takács, E., Wojnárovits, L., 2017. Use of bovine catalase and manganese dioxide for elimination of hydrogen peroxide from partly oxidized aqueous solutions of aromatic molecules—Unexpected complications. Radiat. Phys. Chem. 139, 147–151. https://doi.org/10.1016/j.radphyschem.2017.05.005.
Kovács, K., Simon, Á., Balogh, Gy.T., Tóth, T., Wojnárovits, L., 2020. High energy ionizing radiation induced degradation of amodiaquine in dilute aqueous solution: radical reactions and kinetics. Free. Radic. Res. 54, 185–194. https://doi.org/10.1080/10715762.2020.1736579.
Kovács, K., Simon, Á., Tóth, T., Wojnárovits, L., 2022. Free radical chemistry of atenolol and propranolol investigated by pulse and gamma radiolysis. Radiat. Phys. Chem. 196, 110141. https://doi.org/10.1016/j.radphyschem.2022.110141.
Kovács, K., Tegze, A., Bezsenyi, A., Wojnárovits, L., 2023. Hydroxyl radical induced degradation of the ß-blocker Nadolol and comparison with Propranolol. J. Environ. Chem. Eng. 11, 110330. https://doi.org/10.1016/j.jece.2023.110330.
Kucuki, A., Kadioglu, Y., 2007. Determination of tramadol hydrochloride by using UV and derivative spectrophotometric methods in human plasma. Asian J. Chem. 23, 663–667.
Leresche, F., Torres-Ruiz, J.A., Kurtz, T., von Gunten, U., Rosario-Ortiz, F.L., 2021. Optical properties and photochemical production of hydroxyl radical and singlet oxygen after ozonation of dissolved organic matter. Environ. Sci. Water Res. Technol. 7, 346–356. https://doi.org/10.1039/D0EW00878H.
Li, X., Jenks, W.S., 2000. Isotope studies of photocatalysis: Dual mechanisms in the conversion of anisole to phenol, 2000 J. Am. Chem. Soc. 122 (48), 11864–11870. https://doi.org/10.1021/ja994030h.
Madhavan, V., Schuler, R., 1980. A radiation chemical study of the oxidation of hydroxycyclohexadienyl radical by ferricyanide. Radiat. Phys. Chem. 16, 139–143. https://doi.org/10.1016/0146-5724(80)90220-4.
Mancini, J., Stavagna, C., Pileri, F., Lonardi, G., Arpa, E.M., Galeotti, M., Sisti, S., Juliá, F., Salamon, M., Leonori, D., Bietti, M., 2026. Importance of polar effects in halogen-atom transfer from alkyl iodides to α-aminoalkyl radicals. A kinetic and computational evaluation of the role of structural and medium effects. ACS Au 6, 103–112. https://doi.org/10.1021/jacsau.5c00920.
Manouchehri, A., Nekoukar, Z., Malakian, A., Zakariaei, Z., 2023. Tramadol poisoning and its management and complications: a scoping review. Ann. Med. Surg. (Lond.). 85, 3982–3989. https://doi.org/10.1097/MS9.0000000000001075.
Merga, G., Schuchmann, H.P., Rao, B.S.M., von Sonntag, C., 1996. Oxidation of benzyl radicals by $Fe(CN.\ _6^{3-}$. J. Chem. Soc. Perkin Trans. II 551–556. https://doi.org/10.1039/P29960000551.
Metcalf, L., Eddy, H.P., 2003. Wastewater Engineering: Treatment and Reuse, 4th ed. McGraw-Hill, New York, NY, USA.

Monteil, H., Oturan, N., Péchaud, Y., Mehmet, A., Oturan, M.A., 2020. Electro-Fenton treatment of the analgesic tramadol: Kinetics, mechanism and energetic evaluation. Chemosphere 247, 125939. https://doi.org/10.1016/j.chemosphere.2020.125939.

Moustafa, N.F., Amin, A.S., Diab, M.A., El-Sonbaty, A.Z., Ibrahim, M., 2020. Removing tramadol hydrochloride from wastewater using kaolinite nanocomposite. Egypt. J. Chem. 63, 1397–1409. https://doi.org/10.21608/ejchem.2019.15204.1924.

Nikitin, D., Kaur, B., Preis, S., Dulova, N., 2022. Persulfate contribution to photolytic and pulsed corona discharge oxidation of metformin and tramadol in water. Process. Saf. Environ. Prot. 165, 22–30. https://doi.org/10.1016/j.psep.2022.07.002.

O'Neill, P., Steenken, S., Schulte-Frohlinde, D., 1975. Formation of radical cations of methoxylated benzenes by reaction with •OH radicals, Tl2+, Ag2+, and SO4•− in aqueous solution. Optical and conductometric pulse radiolysis and in situ radiolysis electron spin resonance study. J. Phys. Chem. 86, 2773–2779. https://doi.org/10.1021/j100592a013.

Patel, M., Kumar, R., Kishor, K., Mlsna, T., Pittman, Jr, C.U., Mohan, D., 2019. Pharmaceuticals of emerging concern in aquatic systems: Chemistry, occurrence, effects, and removal methods. Chem. Rev. 119, 3510–3673. https://doi.org/10.1021/acs.chemrev.8b00299.

Plhalova, L., Sehonova, P., Blahova, J., Doubkova, V., Tichy, F., Faggio, C., Berankova, P., Svobodova, P., 2020. Evaluation of Tramadol hydrochloride toxicity to zuvenile Zebrafish—morphological, antioxidant and histological responses. Appl. Sci. 10 (7), 2349. https://doi.org/10.3390/app10072349.

Rózsa, G., Náfrádi, M., Alapi, T., Schrantz, K., Szabó, L., Wojnárovits, L., Takács, E., Tungler, A., 2019. Photocatalytic, photolytic and radiolytic elimination of imidacloprid from aqueous solution: Reaction mechanism, efficiency and economic considerations. Appl. Catal. B Environ. 250, 429–439. https://doi.org/10.1016/j.apcatb.2019.01.065.

Rúa-Gómez, P.C., Guedez, A.A., Ania, C.O., Püttmann, W., 2012. Upgrading of wastewater treatment plants through the use of unconventional treatment technologies: Removal of Lidocaine, Tramadol, Venlafaxine and their metabolites. Water 4, 650–669. https://doi.org/10.3390/w4030650.

Sági, Gy, Bezsenyi, A., Kovács, K., Klátyik, Sz, Darvas, B., Székács, A., Wojnárovits, L., Takács, E., 2018. The impact of H_2O_2 and the role of mineralization in biodegradation or ecotoxicity assessment of advanced oxidation processes. Radiat. Phys. Chem. 144, 361–366. https://doi.org/10.1016/j.radphyschem.2017.09.023.

Sadutto, D., Andreu, V., Ilo, T., Akkanen, J., Picó, Y., 2021. Pharmaceuticals and personal care products in a Mediterranean coastal wetland: Impact of anthropogenic and spatial factors and environmental risk assessment. Environ. Pollut. 251, 116353. https://doi.org/10.1016/j.envpol.2020.116353.

Sarkany, A., Hancu, G., Cârje, A., Papp, L.A., 2019. Chiral separation of tramadol enantiomers by capillary electrophoresis using cyclodextrins as chiral selectors and experimental design method optimization. Chem. Pap. 73, 2363–2370. https://doi.org/10.1007/s11696-019-00789-8.

Schuler, R.H., Hartzell, A.L., Behar, B., 1981. Track effects in radiation chemistry. Concentration dependence for the scavenging of OH by ferrocyanide in N_2O-saturated. aqueous Solut. J. Phys. Chem. 85, 192–199. https://doi.org/10.1021/j150602a017.

Simić, M., Neta, P., Hayon, E., 1971. Pulse radiolytic investigation of aliphatic amines in aqueous solution. Int. J. Radiat. Phys. Chem. 3, 309–320. https://doi.org/10.1016/0020-7055(71)90032-5.

Steenken, S., Neta, P., 1982. Oxidation of substituted alkyl radicals by $IrCl_6^{2-}$, $Fe(CN)_6^{3-}$, and MnO_4^- in aqueous solution. Electron transfer versus chlorine transfer from $IrCl_6^{2-}$. J. Am. Chem. Soc. 104, 1244–1248. https://doi.org/10.1021/ja00369a017.

Stefanic, I., Bonifacic, M., Asmus, K.D., Armstrong, D.A., 2001. Absolute rate constants and yields of transients from hydroxyl radical and H atom attack on glycine and methyl-substituted glycine anions. J. Phys. Chem. A 105, 8681–8690. https://doi.org/10.1021/jp011975o.

Stephan, M.I., 2018. Advanced Oxidation Processes for Water Treatment. IWA Publishing, London. ISBN: 97817804071280.

Subedi, M., Bajaj, S., Kumar, M.S., Mayur, Y.C., 2019. An overview of tramadol and its usage in pain management and future perspective. Biomed. Pharmacother. 111, 443–451. https://doi.org/10.1016/j.biopha.2018.12.085.

Szabó, L., Mile, V., Tóth, T., Balogh, Gy.T., Földes, T., Takács, E., Wojnárovits, L., 2017. On the complex •OH/•O$^-$-induced free radical chemistry of arylalkylamines with special emphasis on the contribution of the alkylamine side chain. Free. Radic. Res. 51, 124–140. https://doi.org/10.1080/10715762.2017.1287356.

Veltwisch, D., Asmus, K.D., 1982. On the reaction of methyl and phenyl radicals with *p*-benzoquinone in aqueous solution. J. Chem. Soc. Perkin Trans. II 1147–1152. https://doi.org/10.1039/P29820001147.

Verlicchi, P., Al Aukidy, M., Zambello, E., 2012. Occurrence of pharmaceutical compounds in urban wastewater: removal, mass load and environmental risk after a secondary treatment-a review. Sci. Total. Environ. 429, 123–155. https://doi.org/10.1016/j.scitotenv.2012.04.028.

Watanabe, T., Honda, K., 1982. Measurement of the extinction coefficient of the methyl viologen cation radical and the efficiency of its formation by semiconductor photocatalysis. J. Phys. Chem. 86, 2617–2619. https://doi.org/10.1021/j100211a014.

Wojnárovits, L., Takács, E., 2013. Structure dependence of the rate coefficients of hydroxyl radical+aromatic molecule reaction. Radiat. Phys. Chem. 87, 82–87. https://doi.org/10.1016/j.radphyschem.2013.02.036.

Wojnárovits, L., Tóth, T., Takács, E., 2020. Rate constants of carbonate radical anion reactions with molecules of environmental interest in aqueous solution: A review. Sci. Total. Environ. 717, 137219. https://doi.org/10.1016/j.scitotenv.2020.137219.

Wojnárovits, L., Homlok, R., Kovács, K., Tegze, A., Takács, E., 2024. Oxidation and mineralization rates of harmful organic chemicals in hydroxyl radical induced reactions. Ecotoxicol. Environ. Saf. 281, 116669. https://doi.org/10.1016/j.ecoenv.2024.116669.

Wolfenden, B.S., Willson, R.L., 1982. Radical-cations as reference chromogens in kinetic studies of one-electron transfer reactions: pulse radiolysis studies of 2,2'-azinobis-(3-ethylbenzthiazoline-6-sulphonate) (II). J. Chem. Soc. Perkin Trans. 805–812. https://doi.org/10.1039/P29820000805.

Wu, D., Hu, Y., Liu, Y., 2022. A review of detection techniques for chemical oxygen demand in wastewater. Am. J. Biochem. Biotechnol. 18 (1), 23–32. https://doi.org/10.3844/ajbbsp.2022.23.32.

Zidane, S., Maiza, A., Bouleghlem, H., Fenet, B., 2019. Inclusion complex of Tramadol in β-cyclodextrin enhances fluorescence by preventing self-quenching. J. Inc. Phenom. Macrocycl. Chem. 93 (3−4), 253–264. https://doi.org/10.1007/s10847-018-0874-1.

Zimmermann, S.G., Schmukat, A., Schulz, M., Benner, J., von Gunten, U., Ternes, T.A., 2012. Kinetic and mechanistic investigations of the oxidation of tramadol by ferrate and ozone. Environ. Sci. Technol. 46, 876–884. https://doi.org/10.1021/es203348q.

Zona, R., Solar, S., 2003. Oxidation of 2,4-dichlorophenoxyacetic acid by ionizing radiation: degradation, detoxification and mineralization. Radiat. Phys. Chem. 66, 137–143. https://doi.org/10.1016/S0969-806X(02)00330-4.